

THE PROGRESSIVE FRAGMENTATION OF 332P/IKEYA-MURAKAMI

KLEYNA, J. T.¹, YE, Q.-Z.², HUI, M.-T.³,
MEECH, K. J.¹, WAINSCOT, R.¹, MICHELI, M.⁴, KEANE, J. V.¹, WEAVER, H. A.⁵, WERYK, R.¹¹Institute for Astronomy, University of Hawai'i at Manoa, Honolulu, HI, 96822, USA; kleyna@ifh.hawaii.edu²Department of Physics and Astronomy, The University of Western Ontario, London, Ontario N6A 3K7, Canada³Earth, Planetary, and Space Sciences, UCLA, Los Angeles, CA 90095⁴ESA SSA-NEO Coordination Centre, 00044 Frascati (RM), Italy and⁵The Johns Hopkins University Applied Physics Laboratory, Laurel, Maryland, 20723, USA

ABSTRACT

We describe 2016 January to April observations of the fragments of 332P/Ikeya-Murakami, a comet earlier observed in a 2010 October outburst (Ishiguro et al. 2014). We present photometry of the fragments, and perform simulations to infer the time of breakup. We argue that the eastern-most rapidly brightening fragment (*F4*) best corresponds to the original nucleus, rather than the initial bright fragment *F1*. We compute radial and tangential non-gravitational parameters, $A_1 = (1.5 \pm 0.4) \times 10^{-8}$ AU day⁻² and $(7.2 \pm 1.9) \times 10^{-9}$ AU day⁻²; both are consistent with zero at the 4 σ level. Monte Carlo simulations indicate that the fragments were emitted on the outbound journey well after the 2010 outburst, with bright fragment *F1* splitting in mid-2013 and the fainter fragments within months of the 2016 January recovery. Western fragment *F7* is the oldest, dating from 2011. We suggest that the delayed onset of the splitting is consistent with a self-propagating crystallization of water ice.

Keywords: comets: individual (332P, P/2010 V1)

1. INTRODUCTION

A comet discovered in PanSTARRS1 (Kaiser et al. 2002) survey data on 2015 Dec. 31 (Weryk et al. 2016) was determined to be the recovery of comet 332P/Ikeya-Murakami (previously known as 332P = P/2015 Y2), which was discovered in 2010 after a massive outburst (Ishiguro et al. 2014). Follow up observations using MegaCam on the Canada-France-Hawai'i telescope (CFHT) on 2016 January 1 showed another comet $\sim 100''$ southwest of 332P. Subsequent observations showed the new comet had many pieces and was undergoing a fragmentation. Sekanina (2016a) suggested that the breakup began in 2010 and that what appeared to be the eastern-most nucleus (our *F2*) is the primary; Sekanina (2016b) argued that a new further-east component (their *C*, our *F4*)¹ is the primary.

We obtained data on 12 nights between 1 January and 10 February 2016, and identified at least 17 fragments, some of which are shown in Fig. 1. The situation is very dynamic with rapid changes in brightness between fragments and new components appearing (fragment *F9* appeared on January 7). Both the initial outburst and this multiplicity of nuclei are observed near perihelion (True Anomaly $TA = 11^\circ$ in 2010; $-44^\circ < TA < 16^\circ$ here.)

Comet splitting may be common, but detailed characterization of a split nucleus is relatively rare. There have been observations of ~ 45 split comets in the last 150 years, with only a handful well studied (Boehnhardt 2004). Splitting is an efficient mass loss mechanism for comets, and is important in their evolution. Two types of splitting are known: (1) splitting into a few pieces, leaving a surviving nucleus; and (2) catastrophic split-

ting into many sub-km fragments. Various mechanisms – e.g., tides, rotation, thermal stress, gas pressure, and impacts – have been proposed for splitting (Boehnhardt 2004), but only in the case of comet Shoemaker-Levy 9 was the mechanism well understood (tidal break up, Sekanina et al. (1994)). Importantly, the size distribution and composition the ejected material can be related to the internal structure of the comet (Belton 2015).

In this paper, we present photometry and astrometry of these central fragments of 332P, and perform dynamical simulations to examine the time span over which 332P broke up. We attempt to use the time of the breakup in relation to perihelion to infer the breakup mechanism.

2. OBSERVATIONS

Our principal observations were obtained with MegaCam on the 3.6m CFHT telescope, on 2016 1 January to 13 April (Table 1). The two initial nights used the *r* filter with exposures of 60s and 90s. Subsequent nights were observed in the more sensitive wide-band *gri* filter for 120s to 180s. Additionally, we obtained *R_C*-band observations with the UH2.2m and Tek2048, on UT 16 Jan 2015 in the middle of the gap between CFHT runs.

Conditions were good on all nights, with little variation in the photometric zero point, and seeing FWHM ranged from 0.7'' to 1.7''.

Figure 1 shows the rapid evolution of the sub-nuclei in relative and absolute brightness, position, and distinctness.

We found additional *i* and *r*-band images in the PanSTARRS1 (PS1) archive from 2015 Oct 10 and 2015 December 4. No evidence of any fragments is seen in October, but fragment *F1* and the *F2* through *F6* cluster are seen in December. Because these are short 45s images on a small 1.8m telescope, it was necessary to stack four images to see the December PS1 *r*-band detections.

¹ Fig. 2 contains a translation of IAU fragment designations to our *F_n* identifiers.

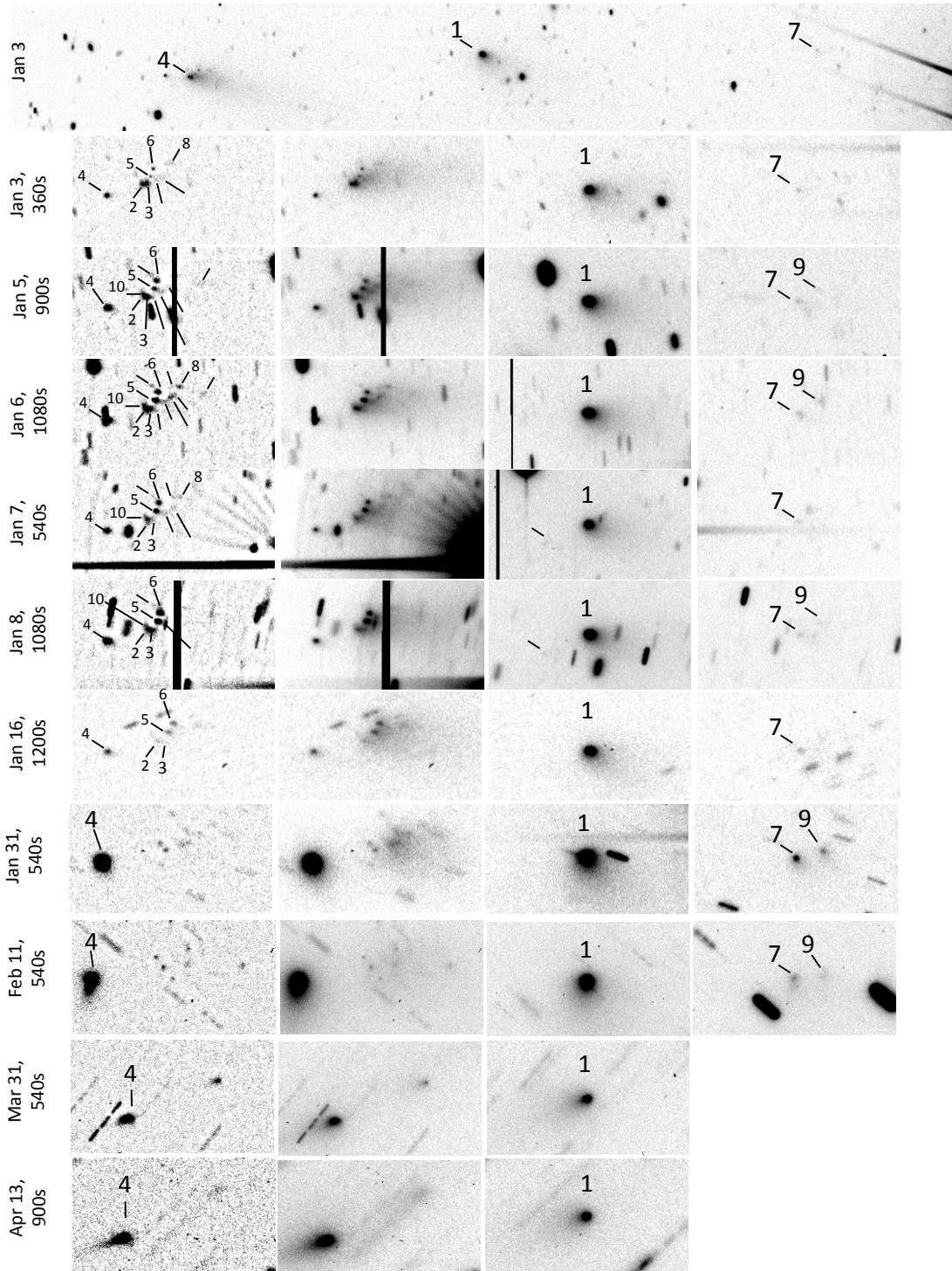


Figure 1. Montage of images of 332P from 2016 January 3 to 13 Apr. The top and bottom strips show a portion of the full image rotated by 21° . Each other (multi-pane) row shows $45'' \times 25''$ regions centered on fragments *F4*, *F1*, and *F7*; N is up and E is to the left. The left column is an enhanced (unsharp mask) view of *F4* to show the fragments. Un-numbered fragments are detected only over a short span of time, and this figure does not show fragments (such as 332P-G) that are far from *F1* and *F4*.

Table 1
Observations

UT Date	UT Times	Telescope/Instrument	Filter	FWHM ^a	No. exp. ^b	Exp. time ^c	r_h ^d	Δ ^e	α ^f	TA ^g
2016-01-01	11:36–11:40	CFHT/MegaCam	<i>r</i>	0.78	3	60	1.73	0.82	18.68	-43.36
2016-01-02	11:30–11:35	CFHT/MegaCam	<i>r</i>	0.74	3	90	1.72	0.82	18.34	-42.86
2016-01-03	13:39–13:44	CFHT/MegaCam	<i>gri</i>	0.69	3	120	1.72	0.81	17.96	-42.30
2016-01-05	13:00–13:16	CFHT/MegaCam	<i>gri</i>	1.12	5	180	1.71	0.79	17.27	-41.29
2016-01-06	12:50–13:09	CFHT/MegaCam	<i>gri</i>	0.75	6	180	1.71	0.79	16.92	-40.78
2016-01-07	13:38–13:46	CFHT/MegaCam	<i>gri</i>	0.90	3	180	1.71	0.78	16.56	-40.25
2016-01-08	10:06–13:14	CFHT/MegaCam	<i>gri</i>	0.91	12	180	1.70	0.77	16.24	-39.77
2016-01-16	08:53–12:01	UH2.2m/Tek2048	R_C	0.93	5	600	1.68	0.73	13.58	-35.57
2016-01-30	09:27–09:35	CFHT/MegaCam	<i>gri</i>	1.53	3	180	1.64	0.67	11.43	-27.87
2016-01-31	11:47–11:55	CFHT/MegaCam	<i>gri</i>	1.50	3	180	1.63	0.67	11.50	-27.25
2016-02-05	09:58–10:06	CFHT/MegaCam	<i>gri</i>	1.51	3	180	1.62	0.66	12.33	-24.44
2016-02-10	10:15–10:23	CFHT/MegaCam	<i>gri</i>	1.72	3	180	1.61	0.65	13.86	-21.54
2016-02-11	10:37–10:45	CFHT/MegaCam	<i>gri</i>	1.63	3	180	1.61	0.65	14.23	-20.95
2016-02-12	10:05–10:13	CFHT/MegaCam	<i>gri</i>	1.69	3	180	1.61	0.65	14.60	-20.38
2016-02-13	10:27–10:34	CFHT/MegaCam	<i>gri</i>	0.73	3	180	1.60	0.65	15.00	-19.78
2016-02-14	06:15–06:23	CFHT/MegaCam	<i>gri</i>	1.58	3	180	1.60	0.65	15.34	-19.30
2016-03-31	06:46–06:54	CFHT/MegaCam	<i>gri</i>	0.70	3	180	1.58	0.81	32.73	8.51
2016-04-05	05:39–05:47	CFHT/MegaCam	<i>gri</i>	0.73	3	180	1.58	0.84	33.76	11.50
2016-04-09	05:36–05:43	CFHT/MegaCam	<i>gri</i>	0.69	3	180	1.59	0.87	34.47	13.90
2016-04-13	06:07–06:26	CFHT/MegaCam	<i>gri</i>	0.70	6	180	1.59	0.90	35.07	16.30

^a Median point source FWHM in arcsec.

^b Number of exposures.

^c Exposure time, in seconds.

^d Heliocentric distance, AU.

^e Geocentric distance, AU.

^f Phase angle, degrees.

^g True anomaly, degrees.

3. PHOTOMETRY

The MegaCam images were bias-subtracted and flattened by the Elixir pipeline at CFHT. We fit a world coordinate system (WCS) using the AstrOmatic SWARP tool (Bertin et al. 2002), and used our custom calibration pipeline to give an absolute magnitude calibration using SDSS DR8 (Aihara et al. 2011). For the r filter, we ignored the minor 1% difference between SDSS r and MegaCam r . For the broadband gri filter, we used a transformation to a gri AB magnitude computed by Simon Prunet (personal communication), where

$$gri_{AB} = -2.5 \log_{10} [0.4388 \times 10^{-0.4g} + 0.4146 \times 10^{-0.4r} + 0.1490 \times 10^{-0.4i}] \quad (1)$$

and g, r and i are SDSS AB magnitudes. Using measurements of fragments $F1$ and $F4$ in a pair of images on 30 Jan, we convert r to gri as $gri = r + 0.18$, and present all photometry.

Because the fragments were crowded, diffuse, and (for $F2$ and $F3$) overlapping, we applied a simple aperture correction to compute individual magnitudes. We computed the magnitude of isolated fragment $F1$ in each image in a large $5''$ diameter aperture, and used this to correct the magnitude of all measured fragments to a smaller $2''$ aperture. Additionally, we increased the size of this calibration aperture inversely with geocentric distance, to maintain a constant physical aperture size. The initially brightest fragment, $F1$, had a magnitude of $r \sim gri \sim 20$, and the faintest fragment $F9$ had $gri \sim 25$.

Figure 2 shows the absolute photometry $m(1, 1, 0)$ obtained by adjusting calibrated magnitude m to geocentric and heliocentric distances $\Delta = r_h = 1$ AU and to phase angle $\alpha = 0^\circ$, with the cometary dust phase coefficient $\beta = 0.02$ derived from Meech & Jewitt (1987) and Krasnopolsky et al. (1987); however Marcus (2007) gives a slightly larger empirical value of $\beta = 0.031$.

$$m(1, 1, 0) = m - 5 \log_{10}(r_h \Delta) - 0.02 \times \alpha \quad (2)$$

The uncertainties shown by the error bars are computed from the scatter of measurements taken during one night.

It is immediately evident that the brightest fragment $F1$ is growing fainter as it approaches perihelion, a trend that is followed by $F2, F3$, and faint fragment $F7$. However, fragment $F4$ appears to rise in brightness in the initial r -band measurements, and $F5$ and $F6$ are growing steadily brighter, suggesting that the cloud is evolving rapidly. Most notably, by 30 January, $F4$ has increased in brightness by two magnitudes, and is clearly the brightest object. On 31 January, its $m(1, 0, 0) \approx 17.5$ is only about one magnitude fainter than the fading value after the 2010 outburst (Ishiguro et al. 2014, Table 2).

In addition to the data in Fig. 2, we performed photometry on the 4 December PS1 images. We measured both fragment $F1$ and the diffuse assemblage at $F2$ to have identical magnitudes $r = 21.9 \pm 0.2$ and $m(1, 1, 0)_{gri} = 17.7 \pm 0.2$. For $F1$ this magnitude is consistent with the dimming trend seen in the subsequent CFHT observations. For $F2$, this value is roughly consistent with the summed flux of $F2, F3, F5, F6$ in the CFHT observations suggesting little evolution in $F1$ or $F2, F3, F5, F6$ from 4 Dec. The surprising result was the complete absence of concentrated fragment $F4$ in the

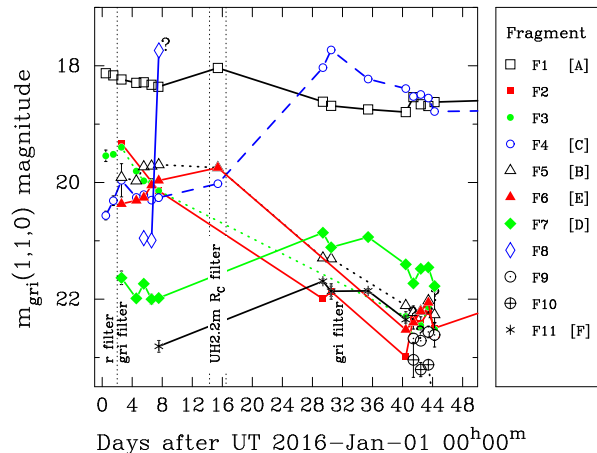


Figure 2. First 50 days of fragment photometry, magnitudes $m(1, 1, 0)$, with a question mark indicating a data point based on a single measurement and near a bright star diffraction spike. r magnitudes of first two nights are converted to gri . With a few exceptions, the error bars are smaller than the graph symbols, omitting systematic uncertainties in the phase correction. The letters in the square brackets in the legend indicate the current CBET and JPL Horizons designations of the fragments; for example, our $F1$ corresponds to 332P-A..

PS1 4 December image. The absence of $F4$ may be consistent with the ongoing brightening as seen in Fig. 2, but may also arise from the depth limitations of the PS1 data.

In a supplementary table to this paper, we present astrometry and photometry of the fragments in Fig. 2 extending to 13 April, omitting the low quality PS1 data. The full data set in the supplementary data table shows fragments $F1$ and $F4$ brightening slightly, and $F2$ brightening by ~ 2 mag.

4. NON-GRAVITATIONAL FORCES FROM ASTROMETRY

The radial and transverse nongravitational parameters, respectively A_1 and A_2 , from a symmetric nongravitational force model devised by Marsden et al. (1973), of component $F4$ were obtained by Hui et al. (in preparation) using EXORB8² to be $A_1 = (1.5 \pm 0.4) \times 10^{-8}$ AU day⁻² and $(7.2 \pm 1.9) \times 10^{-9}$ AU day⁻², taking measurements and astrometry from the Minor Planet Center through UT 2016 April 13, confirming existence of a nongravitational force. $A_2 > 0$ is consistent with prograde rotation (Yeomans et al. 2004). Admittedly the nongravitational model may not be perfectly suitable to the case of component $F4$, as a small but clear systematic bias trend in astrometric residuals starting from 2016 April 09 is identified by Hui et al. However, taking the complexity of the cascading fragmentation experienced by this comet into consideration, and the short observed arc of the 2016 apparition, we think that the application of the nongravitational model is still meaningful.

We also attempted to prove that component $F4$ is the primary component, rather than the earliest detected component $F1$. If the identification of $F4$ as the primary is incorrect, we would expect to see a larger RMS in the orbital solution compared to a correct linkage. By following the same methods and procedures, we set to

² <http://www.sollexorb.it/Sollex120/Download.html>

establish a linked orbit between observations from 2010-2011 and the current observations of component F1. The effort turned out to be very successful and the solution quickly converged after only a few iterations. Indeed, the RMS of the best fit is even slightly better ($\sim 0''.1$) than that of component F4, regardless of ballistic or nongravitational solutions. However, this does not necessarily mean that the identification of component F4 as the primary of comet 332P is erroneous, because the positional uncertainties of F4 are generally greater than those of F1, as a consequence of the well-defined morphology of component F1, and its isolation from any other fragments of 332P. The separation speeds of fragments split off cometary nuclei are generally found to be $\sim 0.1 - 1 \text{ m s}^{-1}$ (Sekanina 1982), which is hard to detect by fitting an impulse from optical astrometric observations alone (Farnocchia, private communication). Therefore the successful linkage between the 2010-2011 observations and observations of component F1 of the current apparition is not surprising. In order to determine the genetic relationship between components F1 and F4, alternative dynamic methods will have to be used.

5. FRAGMENT DYNAMICS

To understand the dynamical properties of the fragments, we make use of the Monte Carlo model developed in our earlier works (e.g. Ye & Hui 2014; Ye et al. 2015, 2016). In detail, our approach creates an ensemble of fragment ejection directions, velocities, and times, and finds those emission events that best match the final observations. Intervals of ejection time that produce a larger number of viable matches with the data are deemed more likely than intervals that produce fewer matches.

The continuing fragmentation of the comet makes it challenging to follow each fragment over an extended period of time, especially for fragments in the debris field surrounding fragment F3. Hence, we focus on four distinct fragments F1, F3, F4 and F7 only. Component F4 is the likely primary as discussed; fragments F1 and F7 are either very bright or distant from the remainder, allowing robust night-to-night associations; fragment F3 began as the brightest fragment in the debris field that was unambiguously followed for the longest time span (2016 Jan. 1 to 8), making it a good representative of the debris field as a whole. All other mini fragments in the debris field are extremely diffuse and it is impossible to uniquely track them for more than a few days.

Unarguably, all fragments are the descendants from the primary component F4. The question is whether all fragments are the *direct* descendants of F4. It is plausible that the fragments continue to split into smaller fragments as already been hinted by the F2-F3 debris field. For a given fragment, any fragment to its east could be its direct parent, i.e. F7 could be the direct descendant of either F1, F3 or F4, and F1 could be directly from either F3 or F4. However, both F1 and F7 are apparently “healthy” fragments while F3 and its immediate companions are only visible intermittently, we feel it is unlikely for F3 (or its direct progenitor) to be the parent of either F1 or F7. Hence, we explore these two scenarios:

1. F4 as the parent of F1, F3 and F7; and

2. F4 as the parent of F1 and F3, while F1 as the parent of F7.

A total of ~ 15 million virtual fragments are released in a 10-day step from the 2010 outburst (circa. 2010 Nov. 1) to the recovery in 2016 (circa. 2016 Jan. 1), from the parent component (either F1 or F4). The fragments are ejected isotropically at random speeds between 0 and 1 m s^{-1} , a range determined by Sekanina (1982). The dynamics of the fragments are then mainly determined by solar gravity as well as the net radial force due to anisotropic outgassing of the respective fragment, described by the ratio between the force and solar gravity, γ (c.f. Sekanina 1977). We then integrate the fragments to the epoch of 2016 Jan. 8.0 TT using the 15th order RADAU integrator embedded the MERCURY6 package (Everhart 1985; Chambers 1999), accounting for the gravitational perturbations from the eight major planets (including the Earth-Moon barycenter), and radiation pressure. At the end, we compare the modeled *relative* positions between the primary and the fragment with the observations, and record the solutions when the observed minus calculated ($O - C$) error is less than $1''$ (roughly one FWHM). Henceforth, we refer this set of solutions as “good” solutions.

The demographics of the “good” solutions are shown as Figure 3 and 4. Fragment direction is expressed in the comet’s reference frame, with the Z axis pointing toward the sun, the orthogonal X axis aligned in the negative orbit direction, and the Y axis pointing north from the XZ orbital plane. A fragment’s ejection direction perpendicular to an assumed spherical surface is specified by standard spherical longitude φ and latitude ϑ . That is, $x = \sin \vartheta \cos \varphi$, $y = \sin \vartheta \sin \varphi$, and $z = \cos \vartheta$. Then $\vartheta = 0^\circ$ points at the sun, $\varphi = 0^\circ$ points in the negative sense of orbital motion, and $\varphi = 90^\circ$ points north.

We immediately note that the solutions do not congregate around or shortly after the 2010 outburst, but instead mostly scatter along the comet’s outbound journey. This indicates that the surviving fragments are not immediately produced by the major outburst. For each fragment:

1. The separation of F1 from the main nucleus most likely occurred in early 2014, with an uncertainty of about 6 months. The median solution is $\vartheta = 120^\circ$, $\varphi = 130^\circ$, split speed $0.5 \pm 0.1 \text{ m s}^{-1}$, and $\gamma \sim 10^{-6}$, representing an emission in the northern hemisphere at the night-side.
2. The split of fragment F3 is complicated by the fact that F3 is observationally less constrained. However, we note that most good solutions congregate over recent epochs, within a few months from the recovery in late 2015, consistent with the fact that fragment F3 is much closer to the primary than fragment F1. This, in turn, implies that the split between F3 and the primary occur much later than the split between F1 and the primary. The good solutions are very scattered across the parameter spaces, but do seem to congregate in the nucleus’ southern hemisphere at the night-side (i.e. $180^\circ < \varphi < 360^\circ$, $90^\circ < \vartheta < 180^\circ$).
3. The simulation favors F4 as the direct parent of

fragment *F7*, as the solution to *F1* leaves a large systematic residual. The split epoch is around late 2011 to early 2012. The median good solutions are near $\vartheta = 90^\circ$, $\varphi = 120^\circ$, or in the twilight zone of the southern hemisphere, with a split speed of $\sim 0.3 \text{ m s}^{-1}$ and a γ of $\sim 10^{-6}$.

In general, our solution agrees with the general conclusion by Sekanina (2016c,d), that all the surviving fragments are likely not immediately produced by the 2010 outburst. Further refinement of split parameters is challenging, as the determination is highly sensitive to the quality of the astrometry. This is especially true for the sub-fragments in the debris field which cross-identification between observations from different night/observatory needs to be done with great care.

6. DISCUSSION

Initially, fragment *F1* was brighter than the nucleus *F4*. However, as noted by Sekanina (1982, 2009), split comet fragment size is often unrelated to dust flux.

The previous far larger outburst of comet 17P/Holmes also produced fragments, but these were seen immediately after the event (Stevenson et al. 2010), in contrast to the 2010 outburst of P/2010 V1. In both events, a proposed mechanism for the outburst was the runaway exothermic conversion of CO-laden amorphous ice to the crystalline form, triggered by a perihelion heat wave from the surface (Sekanina 2009; Ishiguro et al. 2014). It is possible that the delay in fragment emission from the initial outburst is the result of a smoldering ongoing crystallization process initiated by the 2010 perihelion. Fig. 1 of Sekanina (2009) shows that the crystallization process has a many-year slow-growth phase before accelerating catastrophically, in agreement with the delayed fragmentation we observe. If such a process hit pockets of CO rich ice, or if it propagated into deep reservoirs where it reached a critical temperature of $\sim 130 \text{ K}$ months or years later, it could create a sequence of delayed post-perihelion splitting events.

In contrast to amorphous ice crystallization, the direct sublimation of CO or other volatiles, even if they survived at the heliocentric distance of 332P, would be a self-quenching endothermic process.

7. CONCLUSIONS

We performed photometric analysis and dynamical simulations of the central components of fragmented comet 332P. Dynamical arguments indicate that *F4* corresponds to the primary fragment, which is within a magnitude of the $m(1, 1, 0)$ of the fading post-outburst nucleus in 2011.

Dynamical simulations indicate that the breakup occurred over a period of years after the 2010 October outburst, with eastern fragments *F1* and *F7* breaking off as early as 2011.

We thank Simon Prunet for the transformation from g, r, i to the MegaCam gri filter. Q.-Z. thanks Peter Brown for support as well as Paul Wiegert for computational resources. Part of the numerical simulations were conducted using the facilities of the Shared Hierar-

chical Academic Research Computing Network (SHARCNET:www.sharcnet.ca) and Compute/Calcul Canada. We thank Dina Prialnik for useful discussions of the physics of activity, and Eva Lilly for UH2.2m observations. Part of the numerical simulations were conducted using the facilities of the Shared Hierarchical Academic Research Computing Network (SHARCNET:www.sharcnet.ca) and Compute/Calcul Canada. M.-T. thanks Aldo Vitagliano for an improved version of EXORB. RJW acknowledges support by NASA under grants NNX12AR65G and NNX14AM74G. KJM, JK and JVK acknowledge support through the NASA Astrobiology Institute under Cooperative Agreement NNA08DA77A, and partial support through an award from the National Science Foundation AST1413736. MTH is supported by a NASA Solar Systems Observations program to D. Jewitt. Observations were obtained with MegaPrime/MegaCam, a joint project of CFHT and CEA/DAPNIA, at the Canada-France-Hawaii Telescope (CFHT).

Facilities: CFHT (MegaCam), Pan-STARRS1, UH 2.2m

REFERENCES

- Aihara, H., Allende Prieto, C., An, D., et al. 2011, *ApJS*, 193, 29
 Belton, M. J. S. 2015, *Icarus*, 245, 87
 Bertin, E., Mellier, Y., Radovich, M., et al. 2002, in *Astronomical Society of the Pacific Conference Series*, Vol. 281, *Astronomical Data Analysis Software and Systems XI*, ed. D. A. Bohlender, D. Durand, & T. H. Handley, 228
 Boehnhardt, H. 2004, in *Comets II*, ed. M. C. Festou, H. U. Keller, & H. A. Weaver (University of Arizona Press), 301–316
 Chambers, J. E. 1999, *MNRAS*, 304, 793
 Everhart, E. 1985, in *Dynamics of Comets: Their Origin and Evolution*, *Proceedings of IAU Colloq. 83*, held in Rome, Italy, June 11–15, 1984. Edited by Andrea Carusi and Giovanni B. Valsecchi. Dordrecht: Reidel, *Astrophysics and Space Science Library*. Volume 115, 1985, p.185, ed. A. Carusi & G. B. Valsecchi, 185
 Ishiguro, M., Jewitt, D., Hanayama, H., et al. 2014, *ApJ*, 787, 55
 Kaiser, N., Aussel, H., Burke, B. E., et al. 2002, in *Proc. SPIE*, Vol. 4836, *Survey and Other Telescope Technologies and Discoveries*, ed. J. A. Tyson & S. Wolff, 154–164
 Krasnopolsky, V. A., Moroz, V. I., Krysko, A. A., Tkachuk, A. Y., & Moreels, G. 1987, *A&A*, 187, 707
 Marcus, J. N. 2007, *International Comet Quarterly*, 29, 39
 Meech, K. J., & Jewitt, D. C. 1987, *A&A*, 187, 585
 Sekanina, Z. 1977, *Icarus*, 30, 574
 Sekanina, Z. 1982, in *IAU Colloq. 61: Comet Discoveries, Statistics, and Observational Selection*, ed. L. L. Wilkening, 251–287
 —. 2009, *International Comet Quarterly*, 31, 99
 —. 2016a, *Central Bureau Electronic Telegrams*, 4235
 —. 2016b, *Central Bureau Electronic Telegrams*, 4250
 —. 2016c, *Central Bureau Electronic Telegrams*, 4250
 —. 2016d, *Central Bureau Electronic Telegrams*, 4254
 Sekanina, Z., Chodas, P. W., & Yeomans, D. K. 1994, *A&A*, 289, 607
 Stevenson, R., Kleyna, J., & Jewitt, D. 2010, *AJ*, 139, 2230
 Weryk, R., Wainscoat, R.-J., & Micheli, M. 2016, *Central Bureau Electronic Telegrams*, 4230
 Ye, Q.-Z., Brown, P. G., Bell, C., et al. 2015, *ApJ*, 814, 79
 Ye, Q.-Z., & Hui, M.-T. 2014, *ApJ*, 787, 115
 Ye, Q.-Z., Hui, M.-T., Brown, P. G., et al. 2016, *Icarus*, 264, 48
 Yeomans, D. K., Chodas, P. W., Sitarski, G., Szutowicz, S., & Królikowska, M. 2004, in *Comets II*, ed. M. C. Festou, H. U. Keller, & H. A. Weaver (University of Arizona Press), 137–151

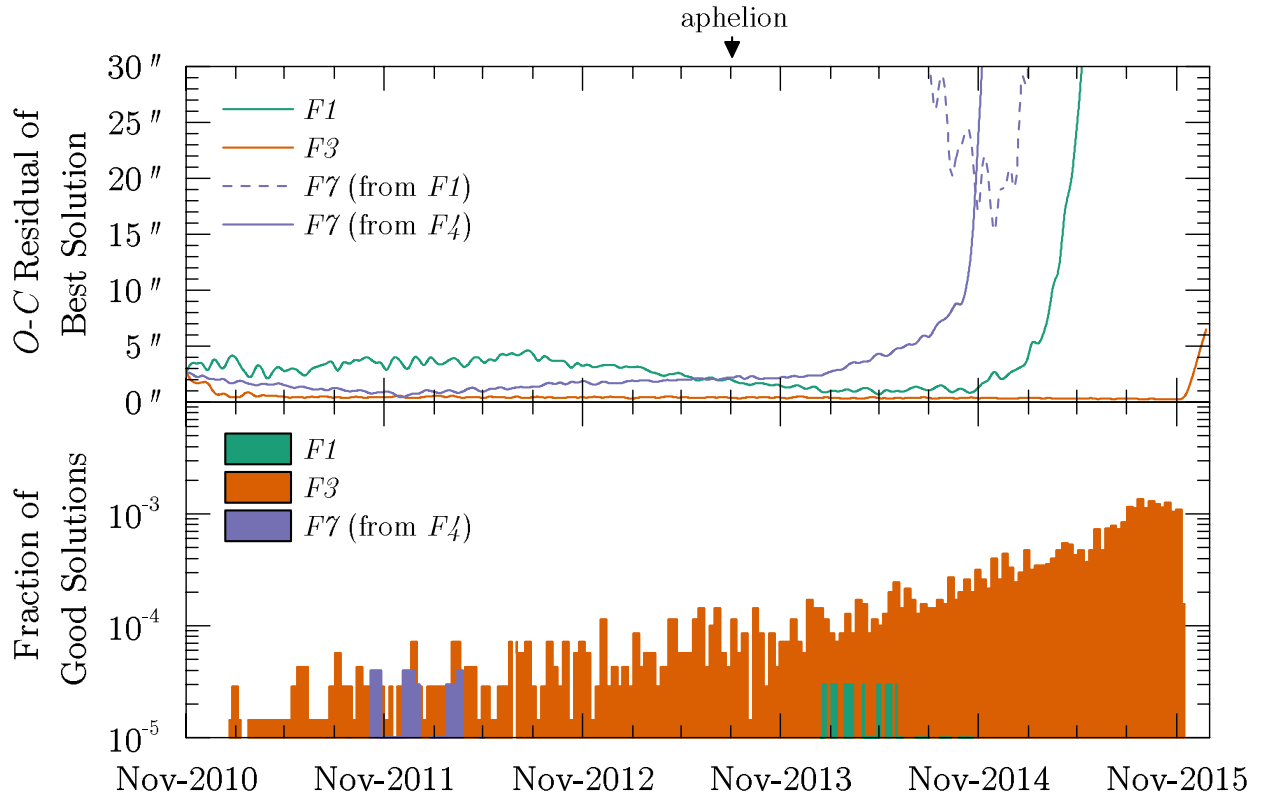


Figure 3. Upper panel: best solutions (i.e. solutions with smallest $O - C$ residuals) at different split epochs; bottom panel: fraction of “good” solutions (i.e. solutions with $O - C$ residual less than half FWHM or $0.5''$). Only those regions of the bottom panel that produce the largest fraction of good detections represent viable ejection times. For example, *F1* (green) could only have been ejected in early to mid-2014.

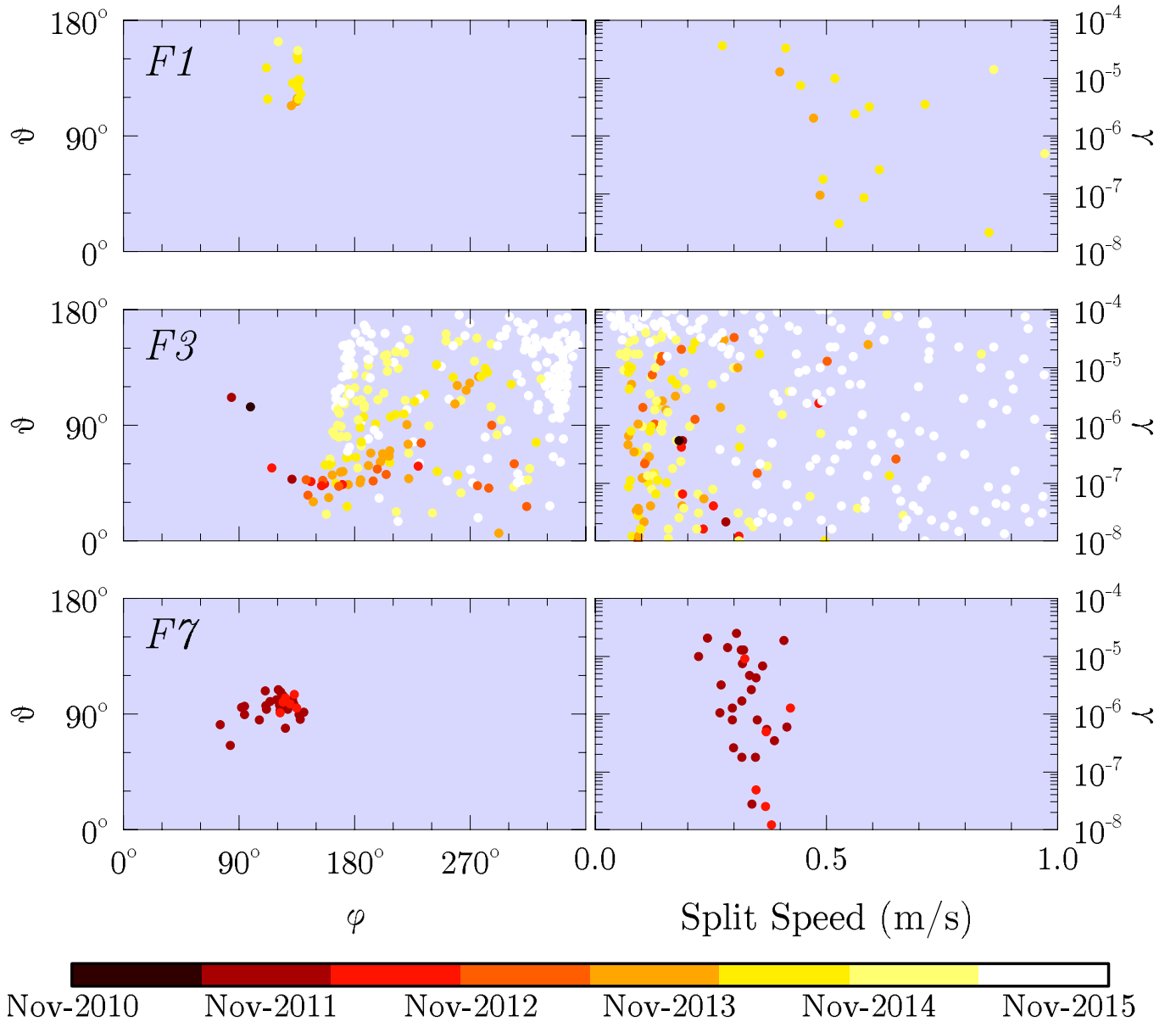


Figure 4. Split direction (left column) as well as split speed and deceleration parameter γ (right column) for good solutions ($O - C$ residuals less than $0.5''$) for fragments $F1$ (upper row), $F3$ (middle row) and $F7$ (bottom row). The data points for fragment $F3$ are under-sampled for clarity. Color denotes different split epoch, filled circle denotes to the scenario that fragment $F4$ is the parent and cross denotes to the scenario that fragment $F1$ is the parent. φ and ϑ are the longitude and latitude in a standard spherical coordinate system, with the Z axis pointing toward the sun, the orthogonal X axis aligned in the negative orbit direction, and the Y axis pointing north from the XZ orbital plane. γ is the ratio of anisotropic outgassing force of the respective fragment to the solar gravity.